Electronic Supplementary Material (ESI) for Physical Chemistry Chemical Physics.
This journal is © the Owner Societies 2018

Supporting Information

Enhanced photocatalytic efficiency of $C_3N_4/BiFeO_3$ heterojunctions: synergistical effects of band alignment and ferroelectricity

Xian-Zhu Deng[a], Chuang Song[a], Yin-Lin Tong[a], Guoliang Yuan[b], Feng Gao[a], Dan-Qing Liu[c,]*, Shan-Tao Zhang[a,]*

[a]National Laboratory of Solid State Microstructures and Department of Materials Science and Engineering, College of Engineering and Applied Science & Collaborative Innovation Center of Advanced Microstructures, Nanjing University, Nanjing 210093, P.R. China

[b]School of Materials Science and Engineering, Nanjing University of Science and Technology, Nanjing 210000, P.R. China

[c]School of Chemical and Environmental Engineering, Harbin University of Science and Technology, Harbin 150040, P.R. China

Corresponding Author

*Email (D. Q. Liu): danqingliu76@163.com

*Email (S-T Zhang):stzhang@nju.edu.cn

Table of Contents:

1. The FT-IR spectra of C_3N_4, $BiFeO_3$, S1, S3, S4 and S5 sample.

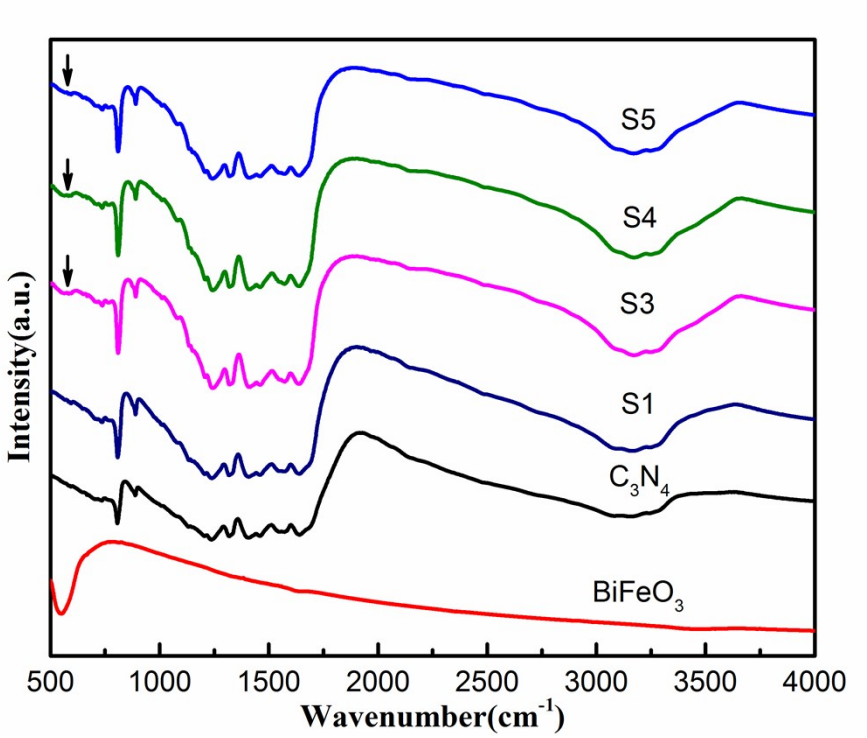

Fig. S1. FT-IR spectra of the g-C_3N_4, $BiFeO_3$ and g-C_3N_4/x$BiFeO_3$ samples. In terms of the g-C_3N_4, the absorption band centered at 806 cm^{-1} is ascribed to s-triazine ring modes. Severe absorption peaks located at 1200-1700 cm^{-1} might result from C-N heterocycles stretching vibrations. The broad absorption band at 3100 cm^{-1} is mainly due to N-H stretching vibrations.[1] In the spectrum of $BiFeO_3$, the absorption peak at 553 cm^{-1} is characteristics of the octahedral FeO_6 groups and result from Fe-O stretching and bending vibrations.[2] As for the g-C_3N_4/*x*$BiFeO_3$ samples (S1, S3, S4, S5, please note S2 has the same composition with S5, so the result of S2 is not demonstrated), the absorption peaks of the g-C_3N_4 exist in all samples, while the absorption peak of $BiFeO_3$ can be observed in S3, S4, S5 samples except S1 sample (indicated by arrow), which is due to the low content of $BiFeO_3$ (10wt.%) in S1 sample.

2. The morphology of C_3N_4, $BiFeO_3$, S1, S2, S3, S4 and S5 sample.

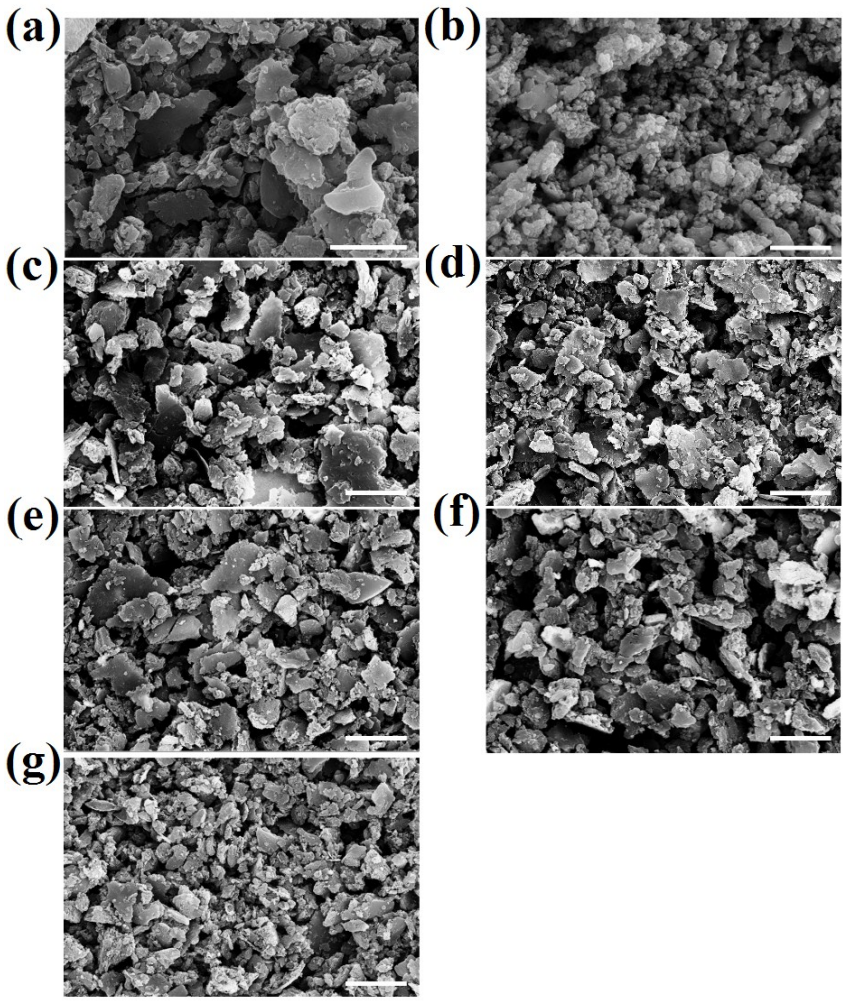

Fig. S2. The SEM images of (a) the g-C_3N_4 (Scale bar, 5 μm), (b) $BiFeO_3$ (Scale bar, 2 μm), and (c~g) g-C_3N_4/*x*$BiFeO_3$ samples (S1, S2, S3, S4, S5, Scale bar, 10 μm), respectively. The morphology of the g-C_3N_4 demonstrates relatively larger anisotropic 2D-like shape characteristics of graphite, whereas $BiFeO_3$ shows a typical isotropic particle shape, some small $BiFeO_3$ particles with size of ~100 nm tend to aggregate into large particle with the size of ~1μm. The relatively larger 2D-like grains in the S1, S2, S3, S4, S5 samples are attributed to g-C_3N_4, whereas some smaller grains are $BiFeO_3$ particles, which are attached to the matrix of g-C_3N_4. It is noted that the S5 sample exhibits the smallest particles with the best size uniformity compared with other g-C_3N_4/*x*$BiFeO_3$ samples, especially compared with the S2 sample which has the same composition. This observation indicates that S5 might have the best photocatalytic performance in our cases.

3. The typical EDS spectrum and the elemental mapping of S5 sample.

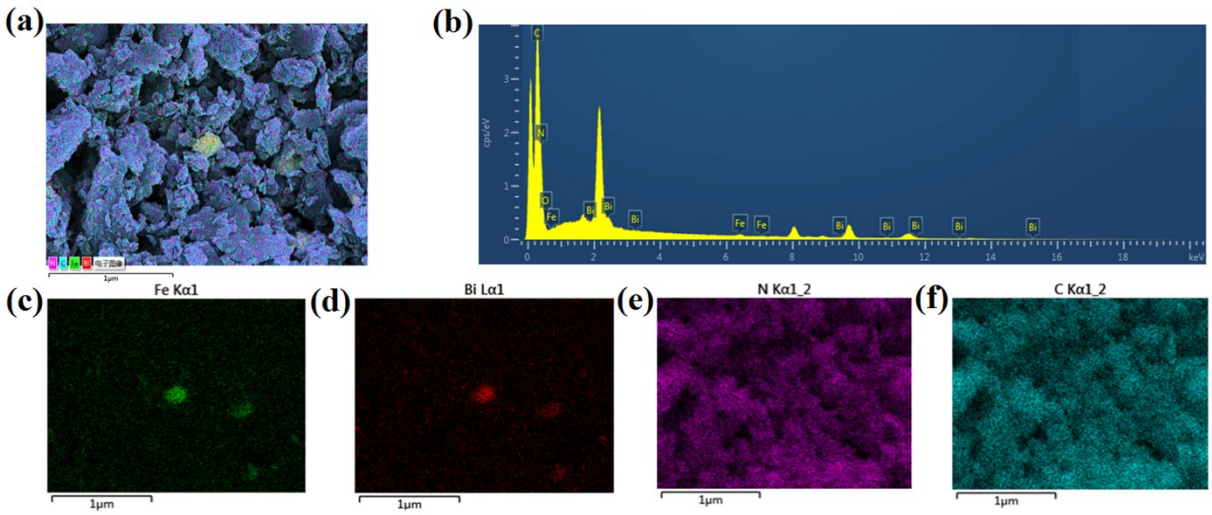

Fig. S3. (a)-(b) The typical EDS spectrum, and (c)-(f) the corresponding elemental mapping images of the S5 sample. The EDS spectrum has shown that the Bi, Fe, C and N elements exist in the S5 sample simultaneously. The elemental mapping images show a homogeneous distribution of C and N, however, the Bi and Fe elements only occupy some isolated regions. This observation suggests that the isolated $BiFeO_3$ particles are embedded in the g-C_3N_4 matrix.

4. The chemical composition of C_3N_4, $BiFeO_3$, S5 and composite sample.

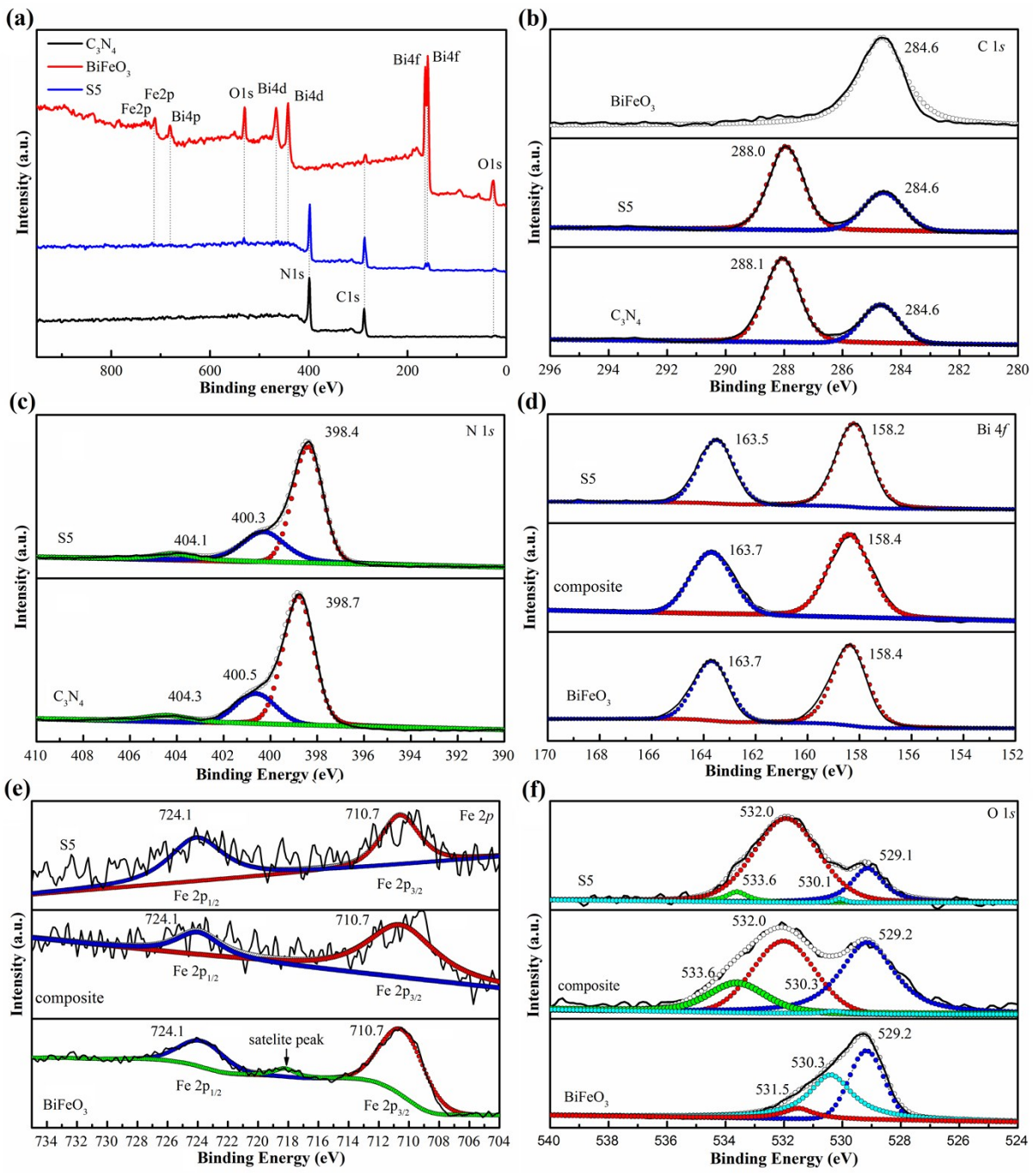

Fig. S4. XPS survey spectra and high-resolution XPS spectra of the C 1s, N 1s, Bi 4f, Fe 2p, and O 1s in the g-C_3N_4, $BiFeO_3$ and S5, respectively. (a) The overall XPS spectra of the g-C_3N_4, $BiFeO_3$ and S5 indicate the existence of C and N elements in the g-C_3N_4, Bi, Fe and O elements in the $BiFeO_3$, and C, N, Bi, Fe, O

elements in the S5. The binding energies were calibrated with respect to the signal from the adventitious carbon (binding energy =284.6eV) (b) the C 1s XPS spectra of the g-C_3N_4, $BiFeO_3$ and S5, the peaks at ~284.6 eV in these three samples result from adventitious carbon of the instrument or the adventitious carbon depositing on the surface of samples. As for g-C_3N_4, the binding energy peak around ~288.1 eV is attribute to the sp^2 hybridized C ($C–(N)_3$). However, this peak in the S5 sample has shifted slightly to 288.0 eV. (c) the characteristic N 1s peak of g-C_3N_4 at 398.7 eV is due to the sp^2-hybridized aromatic nitrogen bonded to carbon atoms (C=N-C). The peak at 400.5 eV is ascribed to tertiary nitrogen ($N–(C_3)$) groups in form of structural motif (C_6N_7) or amino groups carrying hydrogen ($H\text{-}N\text{-}(C)_2$).[3] And the peak at 404.3 eV is assigned to the effects of the charging reaction or the π-excitations. The corresponding N 1s peaks for S5 have shifted to 398.4, 400.3, and 404.1 eV, respectively. (d) the two strong Bi 4f peaks of $BiFeO_3$ at 158.4 eV and 163.7 eV result from Bi $4f_{7/2}$ and Bi $4f_{5/2}$ respectively,[4] the corresponding peaks for S5 have decreased slightly to 158.2 eV and 163.5 eV respectively. (e) The Fe 2p XPS spectra of the $BiFeO_3$ and S5. The two main peaks at 724.1 eV and 710.7 eV of $BiFeO_3$ correspond to the binding energy of Fe $2p_{1/2}$ and Fe $2p_{3/2}$, respectively.[5] It is noted that a satellite peak (~718.3 eV) is 5.8 eV higher than the Fe $2p_{3/2}$ peak, indicating that the chemical state of Fe ion is Fe^{3+} ionic states, but not Fe^{2+} ionic states.[6] However, these peaks fail to appear at the corresponding positions in the Fe 2p XPS spectra of the S5, though some traces of Fe^{3+} could be founded by simulating the XPS spectra. This observation may be mainly due to the low content of $BiFeO_3$ in the S5 sample. (f) The board asymmetric O 1s peaks of $BiFeO_3$ could be deconvoluted into three components. The characteristic peak at 529.2 eV is attributed to Bi-O band, the second peak at 530.3 eV is assigned to Fe-O band,[7] and the third peak at 531.5 eV is ascribed to surface adsorbed hydroxyl groups (O-H).[8] As for the O 1s spectra of the S5, the peak could be deconvoluted into four peaks, the peak at 529.1 eV and 530.1eV can be assigned to Bi-O and Fe-O band.[1,7] The peak at 532.0 eV is ascribed to surface adsorbed hydroxyl groups. The last peak at 533.6 eV is belong to band of C-O in the g-C_3N_4.[7] In general, the shift of the C 1S, N 1s, O 1s and Bi 4f in the S5 sample indicates that intensity interface interaction between the g-C_3N_4 and $BiFeO_3$, i.e., the $C_3N_4/BiFeO_3$ heterojunction is formed.

5. The thermal characterization of C_3N_4/xBiFeO$_3$ sample.

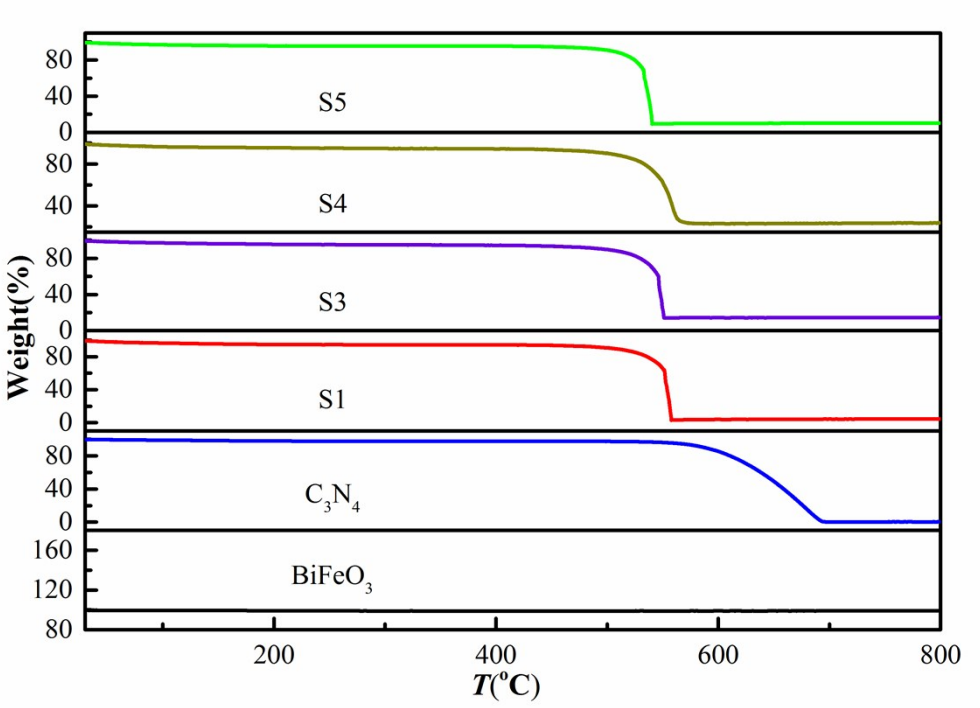

Fig. S5. TG analyses for the BiFeO$_3$, g-C_3N_4, S1, S3, S4, S5 samples**.** The g-C_3N_4 appears thermal decomposition when the temperature is above 694 °C, the BiFeO$_3$ doesn't exhibit thermal decomposition and only shows less than 1% weight loss in the range of 30~800 °C. It is obvious that the thermal stability of g-C_3N_4/xBiFeO$_3$ is decreased as the BiFeO$_3$ is introduced into g-C_3N_4. For example, the sharp weight loss temperature decreases to 557, 540, 551 and 568 °C for the S1, S5, S3, S4 samples respectively. The reason for the decreased thermal stability is that the adsorbing and activating atmospheric oxygen of BiFeO$_3$. The thermal decomposition temperature of S5 is the lowest due to the most uniform distribution of BiFeO$_3$, as evidenced by SEM. It is obvious that only BiFeO$_3$ can be remained when the temperature is above the decomposition temperature of g-C_3N_4/xBiFeO$_3$ samples. Thus, the content of BiFeO$_3$ can be calculated, as listed in the table 1.

6. The N_2 adsorption-desorption isotherms and pore size distributing of g-C_3N_4, $BiFeO_3$, S1, S3, S4 and S5 sample.

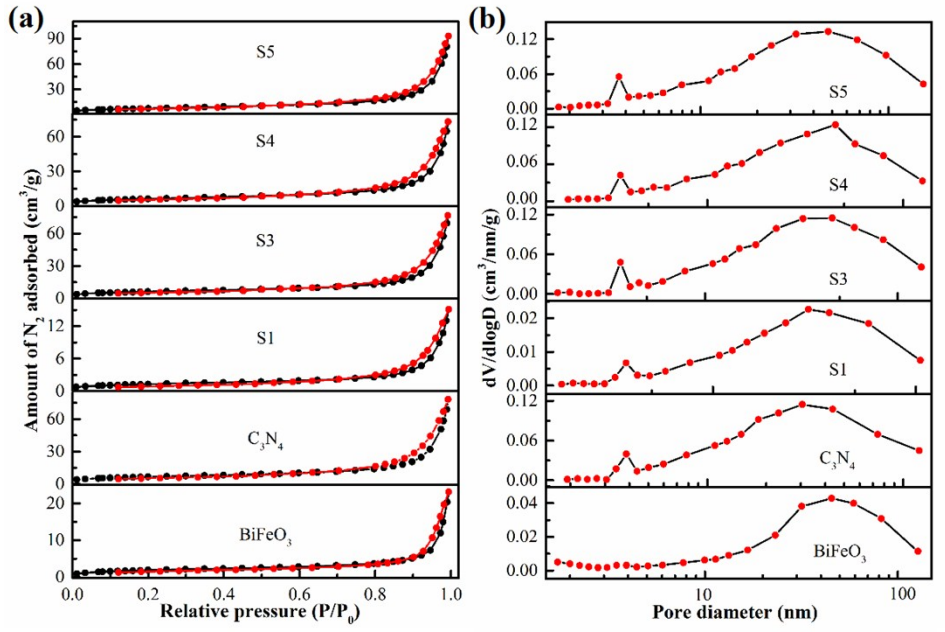

Fig. S6. N_2 adsorption-desorption isotherms and pore-size distribution curves. (a) The Brunauer-Emmett-Teller (BET) specific surface area of the g-C_3N_4, $BiFeO_3$, S1, S3, S4, S5 is calculated to be 24.2, 7.1, 4.7, 22.2, 22.6, 26.8 m^2/g respectively. (b) The pore size distributing of samples are analyzed by the method of Barrett-Joyner-Halenda (BJH). As can be seen, the pore size distribution exhibits two peaks. All samples have a pore size of ~ 3.6 nm except the $BiFeO_3$, and the pore size of $BiFeO_3$ sample is 45.5 nm, furthermore, not only g-C_3N_4 sample but also S1, S3, S4, S5 samples have larger pore size of 31.0 nm, 36.8 nm, 45.6 nm, 45.5 nm and 48.5 nm respectively. All the pores are belonging to mesopores (2~50 nm). Since large pore size and high BET can provide more activity sites for the photodegradation reaction, the S5 sample may have the highest photocatalytic activity due to its largest pore size and BET specific surface area, which is consistent with the structure analysis.

7. Ultraviolet photoelectron spectrum of g-C_3N_4 and $BiFeO_3$.

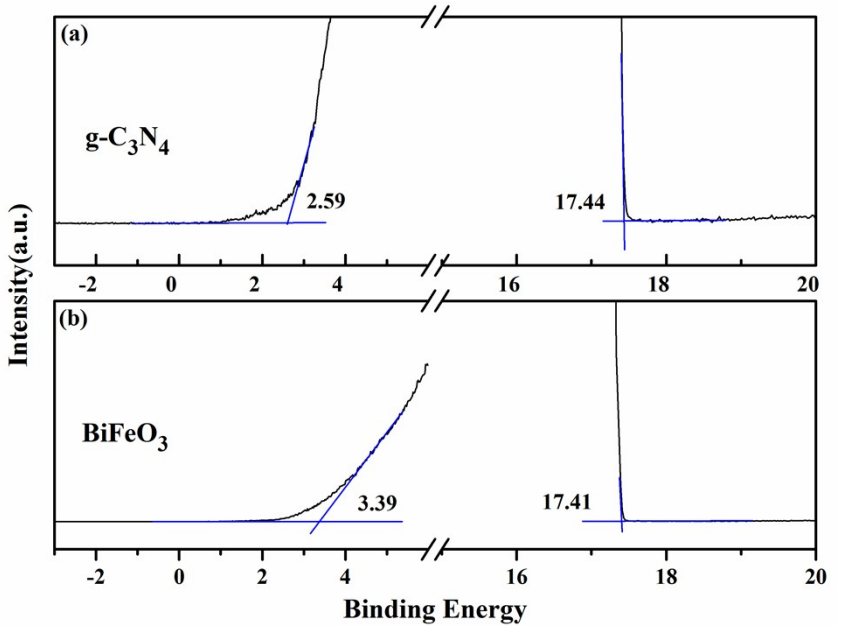

Fig. S7. Ultraviolet photoelectron spectrum as well as linear intersection for (a) g-C_3N_4, (b) $BiFeO_3$. In order to calculate VB and CB potential for g-C_3N_4 and $BiFeO_3$. The UPS of C_3N_4 and $BiFeO_3$ measured at sample biases of -5.0V. The work function of g-C_3N_4 was calculated to be 3.76 eV (vs vacuum) and the corresponding Fermi level (E_F) to be -3.76 eV (vs vacuum). The valence band position (VB) of pure g-C_3N_4 was first estimated to be situated at -6.35 eV (vs vacuum), according to the linear intersection method.[9] By considering that the band gap of C_3N_4 is 2.77 eV, the conduction band (CB) is -3.58 (vs vacuum). Correspondingly, the potentials of E_{VB} and E_{CB} are positioned at 1.91 and -0.86 eV (vs NHE), respectively, based on the relationship between the vacuum energy (E_{abs}) and the normal electrode potential (E_Θ), $E_{abs} = -E_\Theta - 4.44$.[10] Similarly, the value of E_F, E_{VB}, and E_{CB} determined by UV-visible DRS and UPS are summarized in Table S1. As we can be seen, both the E_{VB} or E_{CB} values of C_3N_4 or $BiFeO_3$ are close to their theoretical value.[11]

8. Band energies of g-C_3N_4 and $BiFeO_3$ by UV-visible DRS and UPS.

Table. S1. Band energies of g-C_3N_4 and $BiFeO_3$ by UV-visible DRS and UPS

Sample	E_F		E_{VB}		E_{CB}	
	vs Vacuum	*vs* NHE	*vs* Vacuum	*vs* NHE	*vs* Vacuum	*vs* NHE
C_3N_4	-3.76	-0.68	-6.35	1.91	-3.58	-0.86
$BiFeO_3$	-3.81	-0.63	-7.2	2.76	-5.04	0.6

References:

1 Y. Guo, J. Li, Z. Gao, X. Zhu, Y. Liu, Z. Wei, W. Zhao, C. Sun. *Appl. Catal. B: Environ.* 2016, **192**, 57-71.

2 T. Liu, Y. Xu, S. Feng, J. Zhao, *J. Am. Ceram. Soc*. 2011, **94**, 3060-3063.

3 S. W. Cao, Y. P. Yuan, J. Fang, M. M. Shahjamali, F. Y. Boey, J. Barber, S. C. J. Loo, C. Xue, *Int. J. Hydrogen Energy*. 2013, **38**, 1258-1266.

4 S. Han, C. Sung Kim, *J. Appl. Phys*. 2013, **113**, 17D921.

5 K. Chakrabarti, K. Das, B. Sarkar, S. Ghosh, S. K. De, G. Sinha, J. Lahtinen, *Appl. Phys. Lett*. 2012, **101**, 042401.

6 Mocherla, P. S.; Karthik, C.; Ubic, R.; Ramachandra Rao, M. S.; Sudakar, C. Tunable Bandgap in $BiFeO_3$ Nanoparticles: The Role of Microstrain and Oxygen Defects. *Appl. Phys. Lett*. **2013,** *103*, 022910.

7 Z. Li, Y. Shen, C. Yang, Y. Lei, Y. Guan, Y. Lin, D. Liu, C. W. Nan, *J. Mater. Chem. A*. 2013, **1**, 823-829.

8 H. Li, J. Liu, W. Hou, N. Du, R. Zhang, X. Tao, *Appl. Catal. B-Environ*. 2014, **160**, 89-97.

9 J. C. Wang, H. C. Yao, Z. Y. Fan, L. Zhang, J. S. Wang, S. Q. Zang and Z. J. Li, *ACS Appl. Mater. Interfaces*. 2016, **8**, 3765-3775.

10 G. Xiao, X. Wang, D. Li and X. Fu, *J. Photochem. Photobiol.*, A. 2008, **193**, 213-221.

11 F. Gao, X. Y. Chen, K. B. Yin, S. Dong, Z. F. Ren, F. Yuan, T. Yu and J. M. Liu, *Adv. Mater*. 2007, **19**, 2889-2892.